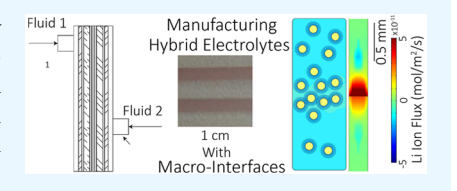


Scalable Manufacturing of Hybrid Solid Electrolytes with Interface Control

Marm B. Dixit, Wahid Zaman, Yousuf Bootwala, Yanjie Zheng, Marta C. Hatzell, and Kelsey B. Hatzell*, Atzell*, Indiana.

Supporting Information

ABSTRACT: Hybrid solid electrolytes are promising alternatives for high energy density metallic lithium batteries. Scalable manufacturing of multi-material electrolytes with tailored transport pathways can provide an avenue toward controlling Li stripping and deposition mechanisms in all-solid-state devices. A novel roll-to-roll compatible coextrusion device is demonstrated to investigate mesostructural control during manufacturing. Solid electrolytes with 25 and 75 wt % PEO-LLZO compositions are investigated. The coextrusion head is demonstrated to effectively



process multimaterial films with strict compositional gradients in a single pass. An average manufacturing variability of 5.75 \pm 1.2 μ m is observed in the thickness across all the electrolytes manufactured. Coextruded membranes with 1 mm stripes show the highest room temperature conductivity of 8.8 \times 10⁻⁶ S cm⁻¹ compared to the conductivity of single-material films (25 wt %, 1.2 \times 10⁻⁶ S cm⁻¹; 75 wt %, 1.8 \times 10⁻⁶ S cm⁻¹). Distribution of relaxation times and effective mean field theory calculations suggest that the interface generated between the two materials possesses high ion-conducting properties. Computational simulations are used to further substantiate the influence of macroscale interfaces on ion transport.

KEYWORDS: hybrid solid electrolyte, scalable manufacturing, ion transport, solid-state battery, process control, coextrusion, interfaces

1. INTRODUCTION

Lithium metal batteries can achieve high energy densities because lithium metal has a high theoretical capacity (3860 mAh/g) and a low reduction potential (3.04 V). 1,2 However, lithium metal suffers from consumptive side effects in liquid electrolytes, and thus solid electrolytes are one approach toward mitigating these effects.³ Solid electrolytes are broadly classified into two material categories: (i) organic (polymer) and (ii) inorganic (ceramic/glass).4-6 Organic solid electrolytes are easy to manufacture into thin films and are mechanically robust and flexible compared to inorganic electrolytes⁷ (Figure 1a). However, these materials possess low ionic conductivities in comparison to inorganic superionic conductors. Inorganic ceramic and glass-type solid electrolytes possess high ionic conductivity, mechanical strength, and electrochemical stability⁸ (Figure 1a). However, processing inorganic solid electrolytes is comparatively difficult. Hybrid electrolytes, which combine organic and inorganic ionconducting materials, represent an emerging family of solid electrolytes that can potentially achieve the advantages of both types of solid ion conductors for scalable applications of solidstate batteries. However, overcoming transport resistances between inorganic and organic phases remains a challenge.

Hybrid electrolytes contain three different material regions: (i) polymer, (ii) inorganic, and (iii) interfacial. The interfacial region is a region adjacent to the inorganic material, which contains disparate material properties (Figure 1b). Ion

transport in these electrolyte systems is fundamentally dependent on the underlying arrangement of inorganic particles within a polymer matrix and the interactions between the two material phases. 10 Hybrid electrolytes demonstrate two percolation thresholds depending on the inorganic phase content: (i) connected particle network at an inorganic loading of >33% and (ii) connected interfacial region at an inorganic loading of <4% (Figure 1b). The addition of inorganic constituents to the polymer matrix leads to Lewis acid-base interactions in the vicinity of the particles. 11 This leads to welldissociated lithium salts that can increase the free Li+ concentration in the vicinity of the particles. Additionally, interactions between the polymer and particles lead to lower polymer crystallinity, which improves the ion transport properties of the polymer. 12-16 Solid-state NMR has shown that ion transport pathways are strongly dependent on the composition of the electrolyte. 17-19 Lithium ions are shown to prefer the plasticizer phase,¹⁷ the ceramic phase in some systems, 19 and transitions from the polymer phase to ceramic phase with some systems. 18 Currently, a knowledge gap exists concerning ion transport pathways in inorganic/organic hybrid solid electrolytes. Furthermore, the confined and nanoscale nature of these solidsolid interfaces makes it experimentally

Received: August 27, 2019 Accepted: November 5, 2019 Published: November 5, 2019



[†]Department of Mechanical Engineering, [‡]Chemical and Biomolecular Engineering, and [§]Interdisciplinary Material Science Program, Vanderbilt University, Nashville, Tennessee 37240, United States

George W. Woodruff School of Mechanical Engineering, Georgia Institute of Technology, Atlanta, Georgia 30313, United States

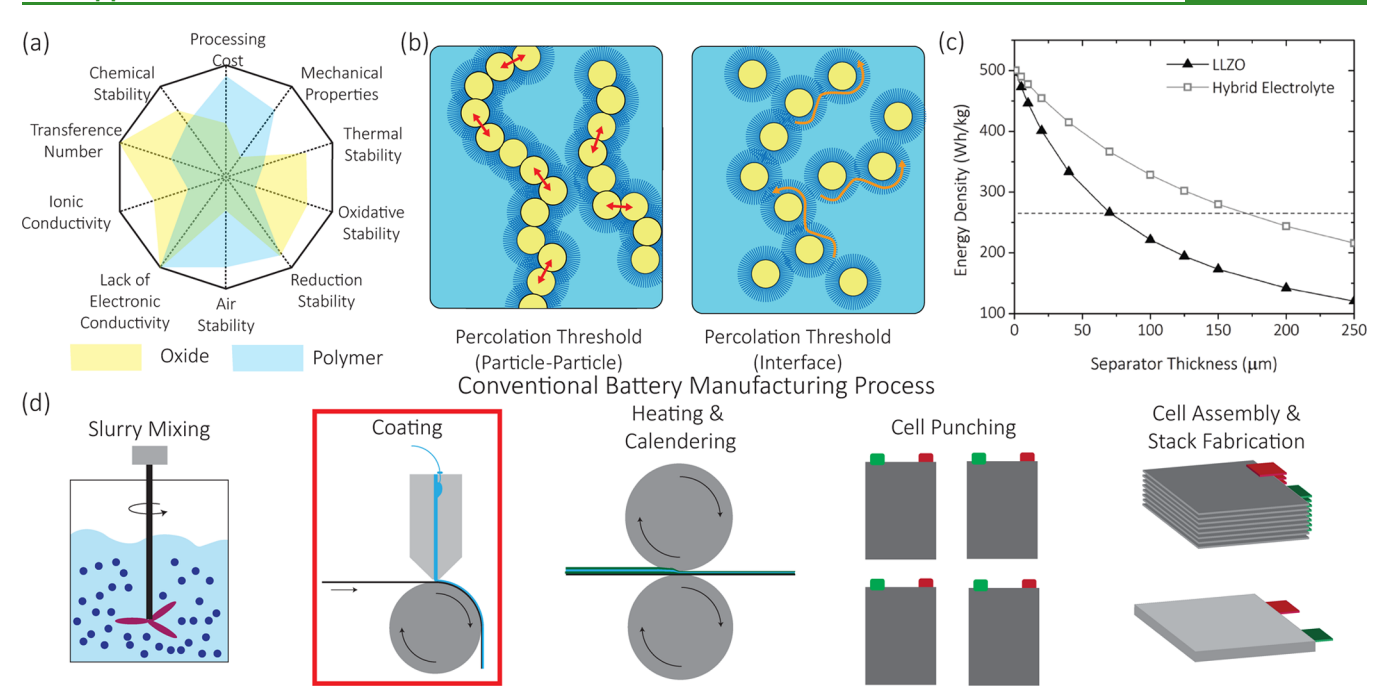


Figure 1. (a) Desired properties for solid electrolytes and relative strengths of oxide and polymer-type solid electrolytes. (b) Gravimetric energy density calculations for LLZO and hybrid electrolytes at 10 mg/cm² cathode loading. An active material/binder/C ratio of 96:2:2 is assumed as the cathode composition. A graphite-NCA-based battery system is considered the state of the art. Energy density calculations are based on the outline provided in ref 9. (c) Particle and interfacial percolation thresholds observed in hybrid electrolytes. (d) Manufacturing process line for conventional liquid-electrolyte-based batteries.

difficult to study. Thus, engineering model systems in order to isolate the organiclinorganic interfaces at a macroscale can provide a way to study ion transport limitations and pathways in hybrid electrolytes.

Aside from transport, scalable manufacturing is one of the most significant challenges facing the adoption of solid-state batteries. 7,20,21 In 2017, there was approximately 3.1×10^9 m² of a separator material manufactured for battery applications.²² This scale demonstrates a large potential market for solid electrolytes and the need for tailored manufacturing processes that can achieve these scales. Solid electrolyte production methods must merge in this existing production chain to ensure economic viability (Figure 1d). Gravimetric calculations show that electrolytes with $\leq 60 \mu m$ (inorganic) and $\leq 160 \mu m$ (hybrid) thicknesses are necessary to achieve energy densities comparable to the state-of-the-art lithium ion batteries (Figure 1c). Furthermore, in order for solid-state batteries to displace the current state of the art, lithium metal anodes are necessary. Currently, nonuniform stripping and plating mechanisms limit the Coulombic efficiency of Li-metal anodes in solid-state batteries. Thus, control over local concentration gradients at solidsoolid interfaces is desired to improve Coulombic efficiencies. One route toward achieving this is through micro- and mesostructural control of solid electrolytes.

Currently, hybrid solid electrolytes are processed from a homogenized dispersion of polymer, lithium salt, and ceramic filler. This dispersion is solution cast onto a polytetrafluoroethylene or Teflon substrate to obtain freestanding films.^{23,24} Electrolytes produced by these methods show ionic conductivities around 10⁻⁵ S cm⁻¹ at room temperature.²⁵ Changing the morphology of the inorganic material has been shown to increase transport properties. For instance, fast ionic conductivity was observed in hybrid electrolytes with inorganic materials with nanowire morphology. 26-29 Changing the

morphology of the conducting inorganic filler modifies the polymer properties in the vicinity of the particles, improving the overall transport. This has been further extended to develop three-dimensional (3D) garnet-polymer frameworks that aim to tailor ion transport through the hybrid electrolvte. 30,31 These 3D frameworks show improved thermal resistance (up to 600 °C) and ion transport properties $(\approx 10^{-4} \text{ S cm}^{-1} \ \text{@ RT})$. The major challenge with tailoring microstructures is achieving control across multiple length scales. Furthermore, contradicting reports suggest that Li ions favor the ceramic phase, the polymer phase, or the interface region, and thus the ideal microstructure is not known. 12-15 For future adoption of hybrid electrolytes, manufacturing processes that can control the arrangement and order of the inorganic phase are necessary.

Herein, a manufacturing platform is engineered to explore the role material interfaces play on transport. This method employs a novel slot die that is compatible with current battery manufacturing approaches. This technique is versatile and can enable control over material composition, density, and structure during roll-to-roll scale processing. This technique can be leveraged toward processing of multimaterial solid electrolytes with tailored microstructural compositions to ameliorate various detrimental interfacial effects in solid-state batteries. We use this platform to engineer macroscale interfaces in hybrid electrolytes to study ion transport through these intrinsic interfaces. In this study, we investigate hybrid solid electrolytes composed of 25 wt % LLZO-PEO and 75 wt % LLZO-PEO. Single-material films and coextruded films with 1 mm (CoX 1mm), 2 mm (CoX 2mm), and 3 mm (CoX 3mm) striped architecture are systematically evaluated for transport and stability (Figure 2c). The configurations and compositions are selected to create hybrid electrolytes with interfaces between a low ceramic containing matrix and a high

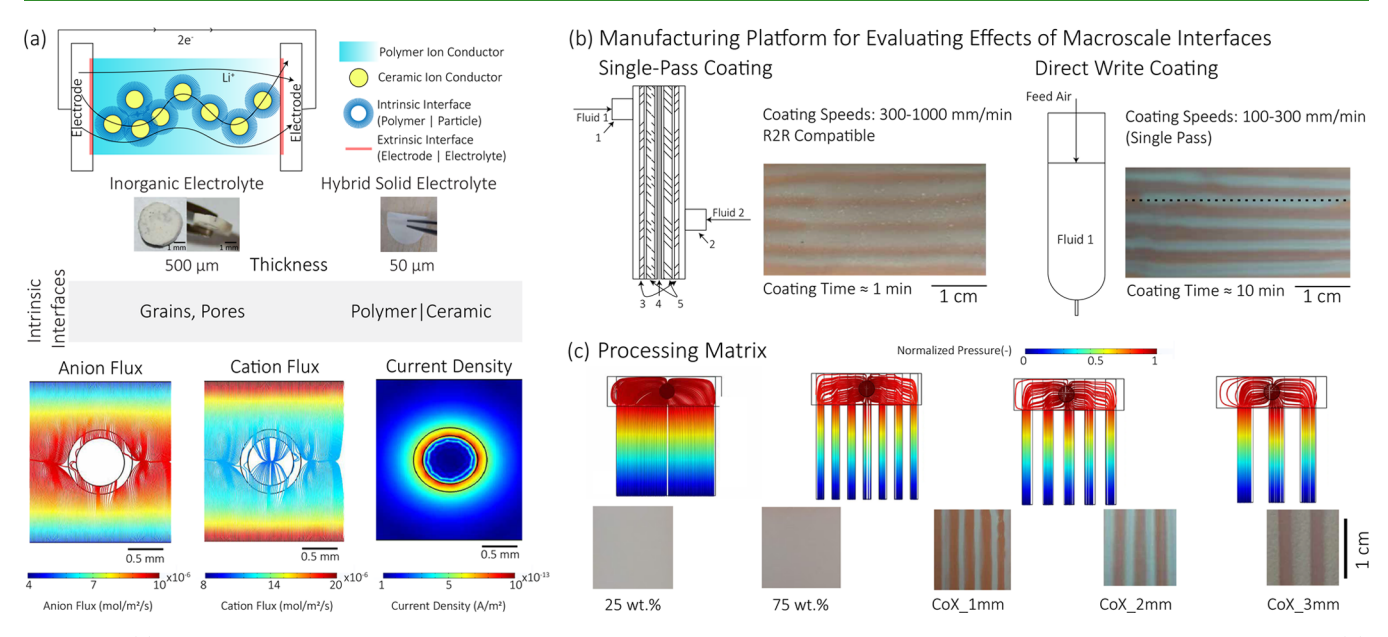


Figure 2. (a) Schematic diagram of interfaces in hybrid electrolytes, ion motion in hybrid electrolytes, and normal current density. (b) Manufacturing platforms for generating hybrid electrolytes with macroscale interfaces. (c) Processing matrix investigated in this study.

ceramic loaded matrix. Coextruded electrolytes show a slight advantage over single-material films, which is attributed to the generation of highly conducting intrinsic interfaces within the hybrid electrolytes. The effect of manufacturing variability on the electrochemical performance of the system is investigated. The nature of these coextruded interfaces is identified using relaxation time distribution of charge transport mechanisms. This is further validated by theoretical modeling of the hybrid system using effective mean field theory and computational modeling.

2. EXPERIMENTAL METHODS

- **2.1. Materials.** Polyethylene oxide (MW: 1,000,000 g/mol) was sourced from Across Organics and used as received. Lithium perchlorate was used as the lithium salt. LLZO was prepared inhouse using a mechanochemical synthesis reported previously.³ A 25 wt % LLZO-PEO system and a 75 wt % LLZO-PEO system are considered as the two primary systems. A required amount of PEO and LiClO₄ was initially dissolved in acetonitrile. An EO/Li ratio was maintained at 18. Subsequently, LLZO was added to the mixture, which was ball-milled in a low energy ball mill until a uniform homogenized mixture was obtained. The total solid loading for both inks was maintained constant at 15 wt %.
- **2.2. Coextrusion Coating.** Two inks are fed pneumatically to the coextrusion die. Single-material films and coextruded films with 1, 2, and 3 mm stripes were manufactured. The architecture of the film was modified by changing the shims within the coextrusion die. A coating speed of 300 mm/min was used. Electrolytes with thicknesses ranging from 50 to 70 μ m have been fabricated using this coextrusion platform. Details of the coextrusion system and integration are reported in the Supporting Information (Figure S1).
- **2.3. Direct Write Coating.** Two inks are fed pneumatically to a regular syringe fitted with a nozzle with an I.D. of 0.5 mm. Striped films are processed by coating the layers for both materials one after the other. A coating speed of 100 mm/min was used. Electrolytes with thicknesses ranging from 50 to 60 μ m have been fabricated using this direct write platform.
- **2.4. Rheology.** Inks used in coating experiments were rheologically studied using a DHR3 Hybrid Rheometer (TA Instruments, USA). All inks were studied using a parallel plate geometry with a 1000 μ m gap thickness. All inks were presheared at 10 s⁻¹ for 10 s and allowed to rest for 5 min prior to any tests to

remove any mechanical history in the samples. Shear sweeps were run from 200 to $0.01~\rm s^{-1}$. Frequency sweeps were run from 0.1 to 600 rad/s. A constant amplitude of 0.1% was applied during oscillating experiments.

- 2.5. Electrochemical Testing. Single films were cast on a copper film for ionic conductivity measurement. After drying, the electrolyte films coated on copper were hot pressed at 100 °C and 400 psi for 1 h. Hot pressing does not result in any change in the architecture of the coextruded membranes (Figure S4). Freestanding electrolyte films were cast on the PTFE substrate for transference number measurement. All electrochemical tests were performed on a VMP3 potentiostat (Biologic, USA). The ionic conductivity of the electrolytes was measured by carrying out AC impedance measurements between 1 MHz and 1 Hz with an amplitude of 10 mV. Transference number measurements were carried out by polarization method in a LilelectrolytelLi configuration. Distribution of relaxation time characterization was carried out for Nyquist impedance spectra obtained at room temperature (see the Supporting Information for technique and fitting details). Galvanostatic charge-discharge studies are carried out on symmetric cells. A constant current of 20 μ A is applied for a duration of 10 min for 50 cycles. Cells are characterized by AC impedance spectroscopy before and after cycling.
- **2.6. Tomography Studies.** Synchrotron X-ray tomography was carried out on the coextruded membranes at 2-BM beamline at the Advanced Photon Source in Argonne National Laboratory. Coextruded samples were held by a metal clip and kept on the rotation stage. 25 keV monochromatic X-rays were used for imaging with a 10× objective lens resulting in an approximately 2×2 mm FOV (field of view) with a resolution of 0.8 μ m. The tomography data was reconstructed using Tomopy. Subsequent image analysis was carried out in ImageJ. Subsequent image analysis was carried out in ImageJ.
- **2.7. Effective Mean Field Theory Modeling.** Effective mean field theory (EMFT) proposed by Li et al.³⁰ is used to predict the properties of the interfacial layer using the known values of ceramic, polymer, and the composite electrolyte conductivity. A very thin interfacial layer ($t \ll R$) is assumed to simplify and aid the estimation. This is a fairly reasonable assumption for the hybrid electrolyte systems under study. The overall equation is given as

$$(1 - f_{c}) \frac{\sigma_{pol} - \sigma_{comp}}{\sigma_{comp} + \text{Li*}(\sigma_{pol} - \sigma_{comp})} + f_{c} \frac{\sigma_{int} - \sigma_{comp}}{\sigma_{comp} + \text{Li*}(\sigma_{int} - \sigma_{comp})}$$

$$= 0$$
(1)

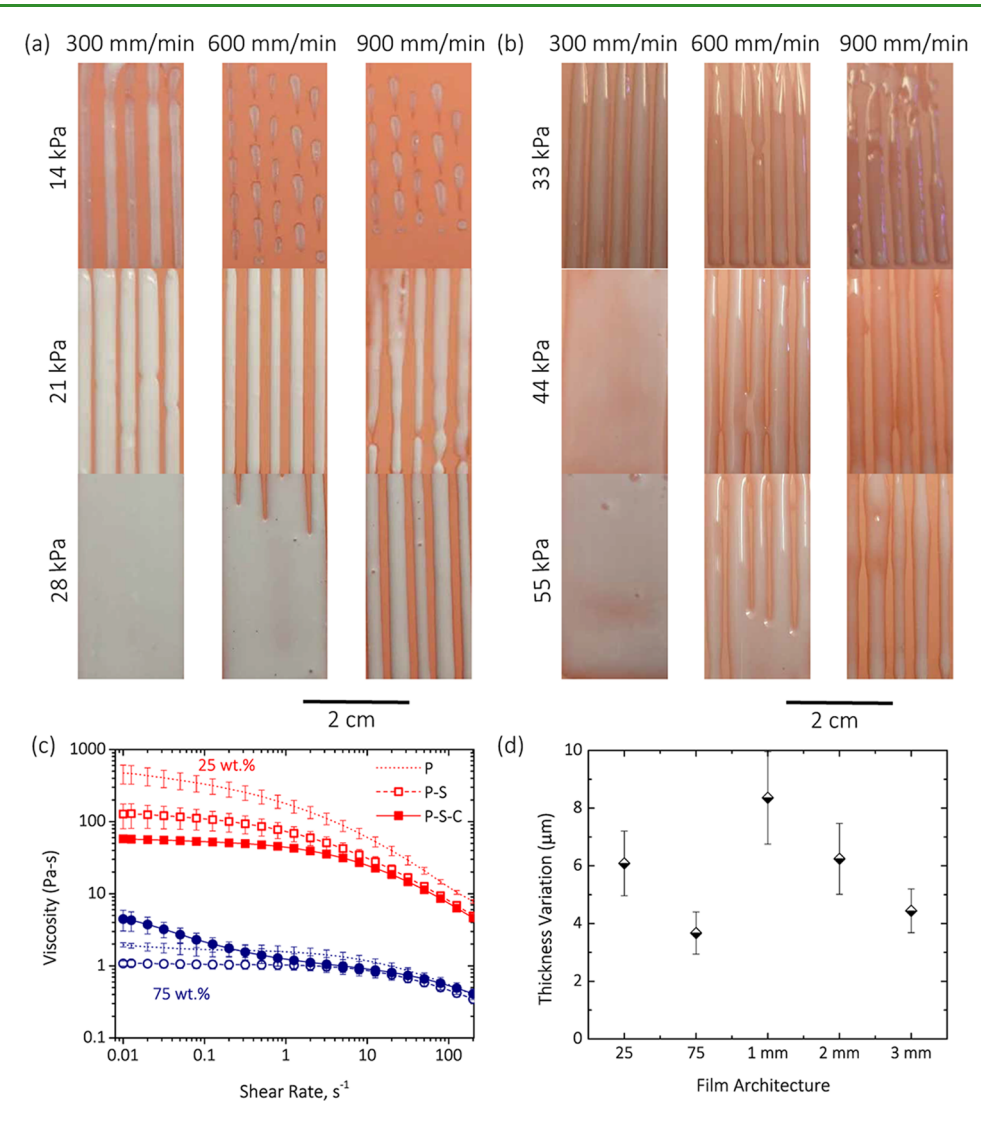


Figure 3. Flow stability analysis for the (a) 75 wt % system and (b) 25 wt % system. Rheology studies for coextrusion inks for solid electrolytes. (c) Steady shear for 25 and 75 wt % LLZO-PEO systems. P, S, and C represent the polymer, salt, and ceramic, respectively. Rheology was measured for the bare polymer ink, polymer-salt mixture, and composite ink. (d) Variation in film heights for different architectures measured using a profilometer. Variations in height are calculated over at least five line scans across the coating at five locations along the coating length.

where σ_{pol} and σ_{int} are the conductivities of the ceramic phase, polymer phase, and the interfacial layer, $\sigma_{
m comp}$ is the effective conductivity of the hybrid electrolyte, and $\sigma_{ ext{eff}}$ is the effective conductivity of the system of the ceramic and the interface. Li* is the effective depolarization factor, and f_c is the volume fraction of the inserted grains. The conductivity of the interface is obtained by solving this implicit equation. Additionally, this model is used to estimate the conductivities of the interfacial region arising within the coextruded system. The detailed derivation of this equation and origins are included in the Supporting Information.

2.8. COMSOL Modeling. 3D simulations are carried out on a 6 mm \times 10 mm electrolyte domain with a 60 μ m thickness. This domain was subdivided into three domains of 2 × 10 mm each. The outer two domains were assigned the physical and electrochemical properties of a 25 wt % system, while the inner domain was assigned the properties of a 75 wt % system. Steady-state flux profiles through the electrolyte are evaluated. A 1 mA/cm² current density is imposed as a boundary condition. Details of the computation model are included in the Supporting Information.

3. RESULTS AND DISCUSSION

There are two types of interfaces that govern ion transport and electrochemical properties in a solid-state system: (i) extrinsic

interfaces and (ii) intrinsic interfaces. Extrinsic interfaces emerge when two materials are integrated together to serve some function, such as an electrodelelectrolyte interface. In contrast, intrinsic interfaces naturally occur in a material or a composite and can affect concentration gradients, degradation pathways, and transport properties. Grain boundaries/voids are examples of intrinsic interfaces or microstructural features in inorganic materials, and organiclinorganic interfaces are examples of intrinsic interfaces in hybrid solid electrolytes. The ionic conductivity is lower in hybrid electrolytes than inorganic electrolytes and is often attributed to a formed interfacial resistance $(R_{\rm int})$ at the polymerlceramic interface, $^{34-36}$ which prevents transport between the two materials (Figure 2a).³⁷ Phenomenologically, this can be seen when mapping anionic and cationic flux in the polymer, ceramic and interfacial regions respectively using effective mean field theory (Figure 2a). Ceramic electrolytes have a lithium ion transference number close to one, effectively blocking all anion transport. Ceramic electrolytes have a lithium ion transference number close to the one that blocks all anion transport. This leads to redistribution of anions over the particles and higher

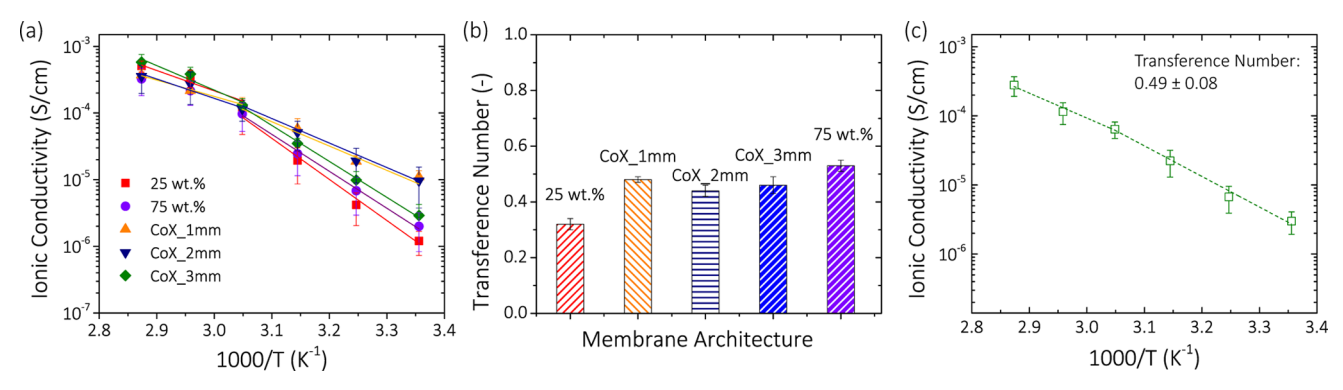


Figure 4. (a) Ionic conductivity and (b) transference number of coextruded membranes. (c) Ionic conductivity and transference number of membrane processed using the direct write protocol.

effective current densities in the interfacial region (Figure 2a). Thus, control over organiclinorganic interfaces during manufacturing may provide a means for directing ion transport to extrinsic interfaces (electrode). Uniform and controlled concentration gradients are important in order to mitigate degradation phenomena accelerated by the formation of local hot spots and/or lithium metal pore formation (i.e., Li excess/ deficient regions).

Slot die coaters are extensively used in roll-to-roll manufacturing.³⁸ Conventional slot die instruments contain flow dividers and a shim in order to control the coating fluid and coating area. Furthermore, precise mass flow regulation is necessary to maintain coating resiliency during a manufacturing pass. The coextrusion (CoX) printhead designed is an extension of a conventional slot die head (Figure 2b and Figure S1a,b). The CoX head is capable of coating two layers in a single pass. Fluid one is connected to the inlet port one (1), and fluid two is connected to inlet port two (2). In the interior of the CoX head, the fluid is distributed across the width of the CoX head by using a flow divider (3). Subsequently, specially designed shims (4) channel the flow in multiple configurations. The mixing of two fluids is prevented by a flow separator (5). The CoX head can deliver single-material coatings and multimaterial coatings with through-plane or in-plane gradation. The exact configuration is dependent on the CoX head setup and processing parameters. Similar control over local architectures is obtained by direct write coating techniques, which is adapted from the 3D printing domain (Figure 2b). The coextrusion platform is capable of coating areas of up to 200 cm²/s. Direct write coating is significantly more time-consuming, taking up to 10 times more time for coating the same areas (Figure 2b). To ensure a uniform pressure distribution at the outlet of the CoX head, the flow dividers and the shims were designed using computational fluid dynamics simulations as a design tool. Flow divider geometry and shim configurations are designed to achieve a uniform pressure distribution at the exit (Figure 2c). The pressure at the exit of the flow patterns is fixed at ambient conditions, and simulations are carried out at a range of viscosities (ink formulations) and inlet pressures. Typical flow patterns and pressure distribution show a uniform flow at the exit for all the configurations with a uniform pressure at the outlet. This results in optimum flow paths for the two fluids resulting in well-defined coextruded films, as evidenced in the optical images. Optical pictures and tomography reconstruction also show the striated nature of the coextruded membranes (Figure

2c and Figure S1c,d). It is important to note that all the individual configurations are obtained in a single pass coating.

The coating stability window of different ceramic/polymer inks (25 and 75 wt %) was systematically investigated (Figure 3a,b). A stable coating is obtained when the coating bead forms stable liquid—vapor interfaces with its environment (Figure S2).^{39–42} If the pressure inside the bead is too large, then the ink swells out in all directions, leading to a defect called leaking. This defect leads to loss of control over the coating width and thickness. At the other extreme, if the pressure in the bead is too low, then air can entrain in the film at the upstream meniscus, leading to break up of the coating bead. The defect begins at isolated spots and can deteriorate into uncoated streaks. At very high web speeds, the downstream meniscus can break up and lead to uncoated regions through the width of the slot and can manifest as ribbing/ripples in the coating. At 14 kPa and 300 mm/min, the 75 wt % ink shows poor coating behavior due to a low mass flow rate. At 600 and 900 mm/min, the coating bead loses contact with the substrate and ribbing behavior is seen. At 21 kPa, 300 mm/min shows evidence of leaking behavior due to low coating speeds and higher mass flow rate. A 600 mm/min speed shows a clearly coated stripes, while the stripes again show ribbing behavior at 900 mm/min. At 28 kPa, leaking behavior is seen at all coating speeds; however, it reduces with increasing coating speed. Similar observations can be made about the 25 wt % (ceramic/polymer) ink. The coating pressure for both inks and the coating speed were obtained by carrying out this parametric study.

Rheological experiments are used to investigate the flow behavior of the respective inks (Figure 3c and Figure S3a). Effective coating is dependent on having uniform material properties during coating. 43-50 Both of the inks used for coextrusion show shear thinning behavior in the regime of interest $(1-100 \text{ s}^{-1})$. The viscosity of the 75 wt % (ceramic/ polymer) ink is 2 orders of magnitude lower than that of the 25 wt % ink (22.63 vs 0.87 Pa·s at 12 s⁻¹). Thus, since the two inks demonstrate different rheological properties, there is a need for different operating pressures during coextrusion (Figure S1a,b). The addition of a salt (Li source) reduces the viscosity of a pure polymer solution. Salt introduces chargescreening effects in the polymeric solution, leading to a reduced repulsive force in the polymer chains.⁵¹ This leads to a reduction in the hydrodynamic radius of the polymer and the degree of polymer chain entanglement. Together, these factors lead to a reduction in the polymer viscosity. Subsequently, the addition of ceramic particles also reduces the viscosity for the

Table 1. Activation Energies (eV) for Ion Transport

hybrid electrolytes					
branch	25 wt %	75 wt %	CoX_1mm	CoX_2mm	CoX_3mm
low temperature	0.53	0.48	0.32	0.31	0.46
high temperature	0.26	0.26	0.21	0.25	0.32
interfaces					
branch	25 wt %	75 wt %	CoX_1mm	CoX_2mm	CoX_3mm
low temperature	0.42	0.43	0.25	0.21	0.46
high temperature	0.27	0.19	0.14	0.21	0.37

25 wt % system due to further chain disentanglement. An increase in viscosity is seen in the low shear region, indicating a percolated particle network for the 75 wt % ink (ceramic/ polymer). Both systems show a higher loss moduli than storage moduli, suggesting the presence of unstructured agglomerates (Figure S3a).

Quality control is of significant interest in battery manufacturing because irregularities will lead to variable material properties. 52-56 Thus, it is imperative to analyze the process variability in the manufacturing process. Profilometry studies were carried out on coextruded electrolytes across multiple sections along the length of coating. The average thickness variation in the different coextruded electrolytes is reported (Figure 3d and Figure S3b). The average variation across all the samples is $5.75 \pm 1.2 \,\mu\text{m}$. This error is within the resolution limits of the gantry stage used for the coextrusion system (± 50 , ± 150 , and $\pm 10 \mu m$ in the *X*, *Y*, and *Z* direction). Moving to a dedicated coating platform with improved motor resolution and better load management can improve the variability response of the coextrusion system. The thickness variations observed here are ≈5-10% of the average electrolyte thickness.

Electrochemical properties for the coextruded and singlematerial films were systematically investigated (Figure 4a-c). The ionic conductivities for the 1, 2, and 3 mm coextruded samples were similar for temperatures between 25 and 70 $^{\circ}\text{C}$ (Figure 4a) and larger than the single-material electrolytes. For statistics and quality control, 10 separate samples were measured. Detailed results with errors are reported in the Supporting Information (Tables S1-S5). The ionic conductivities reported here are generally on the lower side with a room temperature conductivity of $\approx 10^{-5}$ S cm⁻¹ for the coextruded membrane. Employing strategies like optimal loading of ceramics, ^{10,23} addition of plasticizer, ¹⁷ tailoring polymer composition, ¹¹ or moving to a bulkier anion ²⁶ can help improve the ionic conductivity values. Model PEO-LiClO₄-LLZO inks were used for this proof-of-concept study that exhibited distinct composition and rheological properties. The relatively large spread seen in the ionic conductivity data can arise from the variability in processing discussed earlier. Even so, an improvement in the mean value of ionic conductivity is observed for coextruded membranes compared to single-material films (Figure 4a). The activation energy (measured on the average data) also shows an equivalent decrease for the coextruded configurations compared to the single-material films below the transition temperature of the polymer (Table 1). The striped architecture resembles a parallel conductor network for which the equivalent conductance is equal to the sum of individual conductance in the circuit. Charges are redistributed through the individual stripes to minimize the voltage drop across the system. The equivalent

circuit model described above considers electron motion, which is not the case for the hybrid electrolytes. Ion transport through the electrolyte is limited by kinetics of ion motion through the material. Increases in ionic conductivity for coextruded solid electrolytes suggest that the addition of macrointerfaces facilitates transport pathways within the electrolyte that possesses better ion transport kinetics. Generally, in hybrid electrolytes, improved ion transport is ascribed to (i) increased ion-pair dissociation, (ii) enhanced Li⁺ surface transport, (iii) anion attraction at the inorganic phase surface due to Lewis acid-base interactions, (iv) polymer chain-promoted surface transport, and (v) improved ion transport through the polymer phase due to reduced crystallinity.⁷ The architectures designed for this study are tailored so that the microstructure at the interface between the low loading ink and high loading ink is distinct than that between the respective bulk systems. This region can be identified as the macrointerfacial region between the two coextruded regions. The distribution of the organic, inorganic, and so-called space-charge layer will be distinct from the bulk materials. The results suggest that this redistributed interfacial region between the two systems is likely the cause of improvement in the ionic conductivity. The mechanism for improved ion transport rates is likely to be described by a combination of the factors discussed above. It is extremely difficult to evaluate mechanistic information about ion transport experimentally, and modeling techniques are used to provide insight into the interfacial mechanisms for improved ion transport.³⁷ It is understood that manufacturing platforms with a higher resolution and better load management can overcome the process variation seen in this study and showcase the improvement in the coextruded electrolytes more effectively. However, the current platform demonstrates clearly the potential value for multimaterial manufacturing as a means to control electrochemical and transport properties in a part or component.

Transference number is another electrolyte property that dictates the electrochemical performance. ^{57–59} High transference number electrolytes minimize the concentration and polarization gradients, improve power performance, and mitigate the risk of catastrophic failure via shorting due to uniform concentration profiles. The transference number of the uniform coating with 25 wt % ceramic is 0.36, while the transference number of the uniform coating with a 75 wt % system is 0.56 (Figure 4b). Addition of ceramic particles to the polymer matrix improves the Li-salt dissociation and mobility of Li⁺ due to charge screening.⁶⁰ Improved salt dissociation and anion immobilization on increasing the single ionconducting inorganic phase fraction leads to a higher transference number for the 75 wt % system. The transference number for the coextruded electrolytes falls between these two

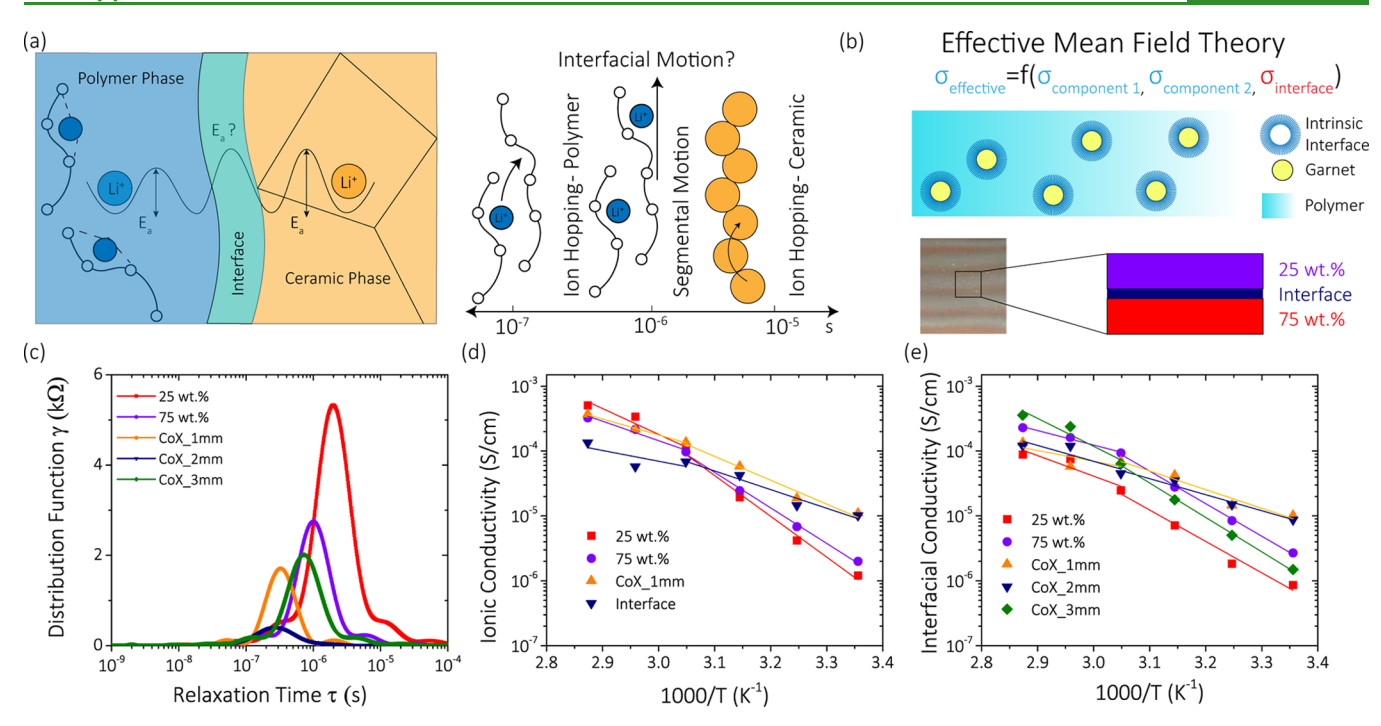


Figure 5. (a) Schematic diagram of Li ion transport in hybrid electrolytes with ion transport mechanisms and characteristic time scales. (b) Effective mean field theory model for estimating interfacial properties. (c) Distribution of relaxation time results for all samples. (d) EMFT results for the CoX 1mm membrane with 25 and 75 wt % systems as the bounding components. (e) Interfacial conductivities for all samples.

systems. According to the concentrated solution theory, 61 the cation transference number is related to the effective diffusion coefficients of the binary salt in the medium, which in turn depends on the conductivity.⁶² The experimental results show an improved ionic conductivity for the coextruded films; however, the transference number remains between the two boundary systems. This indicates an equal improvement in both anion and cation diffusion coefficients, which results in a higher conductivity but an effectively averaged transference number. There can be several competing mechanisms occurring at the macrointerfaces that can lead to this behavior, including anion immobilization, charge screening, and ion redistribution. Further investigation into the differences in the bulk and interfacial microstructure and chemical morphology is

In order to test the hypothesis that the improved transport is ascribed to the macrointerfaces and not process-related parameters, we tested a similar striped architecture using direct writing printing. These are another approach capable of generating architectures similar to the coextrusion system. The primary difference between direct write and coextrusion manufacturing platforms is the speed of processing. Coextrusion coats multiple inks at the same time and thus is much more facile for high-throughput processing. However, there is a possibility of mixing at the interfacial region in coextrusion manufacturing. Diffusion of components within the two ink stripes during the drying step can also occur due to the composition difference between the two inks. These phenomena have less impact with the direct write coating process. The ionic conductivity of the direct write striped electrolyte shows a slightly higher conductivity than the singlematerial electrolytes (75 and 25 wt %) and median transference number values (4.12 \times 10⁻⁴ vs 3.98 \times 10⁻⁴ S cm^{-1} (25 wt %) and 2.21 × 10⁻⁴ S cm⁻¹ (75 wt %)). The coextruded electrolyte with a similar stripe configuration (2

mm) shows slightly higher ionic conductivities $(6.31 \times 10^{-4} \text{ vs})$ 4.12×10^{-4} S cm⁻¹ @ 75 °C) and smaller activation energies (-0.966 vs -1.06 eV). These results suggest that the macroscale interfacial regions are responsible for the enhanced ion transport properties.

Deconvoluting the ion transport mechanisms between the polymer phase, ceramic phase, and the interfacial region is challenging (Figure 5a). Intra- and interchain ion hopping mechanism and segmental motion of the polymers are known transport mechanisms through the polymer phase (Figure 5a). Li transport in the garnet occurs primarily through hopping mechanisms that are driven by vacancy concentrations in the crystal structure. The improved ionic conductivity and median transference number suggests that the transport mechanisms at the interfacial regions is through a confined polymer matrix. Multiscale modeling of battery materials is an effective tool to deconvolute experimental results. We employ distribution of relaxation time analysis as an experimental approach toward deconvoluting the ion transport mechanisms in these coextruded systems. This is complemented by theoretical modeling using effective mean field theory (Figure 5b) and three-dimensional fluid dynamics simulations (Figure 6).

Distribution of relaxation time is a method for deconvoluting transport mechanisms from impedance spectra. 63,64 This technique does not require any a priori assumptions regarding the system behavior as is necessitated in equivalent circuit modeling of the impedance spectra. Furthermore, this technique can distinguish between mechanisms with similar time constants. The distribution relaxation time spectra of the single-material 25 wt % solid electrolytes show one primary peak at $\approx 2 \times 10^{-6}$ s and shoulders at $\approx 1.3 \times 10^{-5}$ and 3.0 \times 10⁻⁷ s. These may represent the characteristic ion transport mechanisms in the polymer: inter- and intrachain ion hopping and segmental motion, respectively. The ceramic concentration at this loading is ≈7 vol %, which suggests a discrete

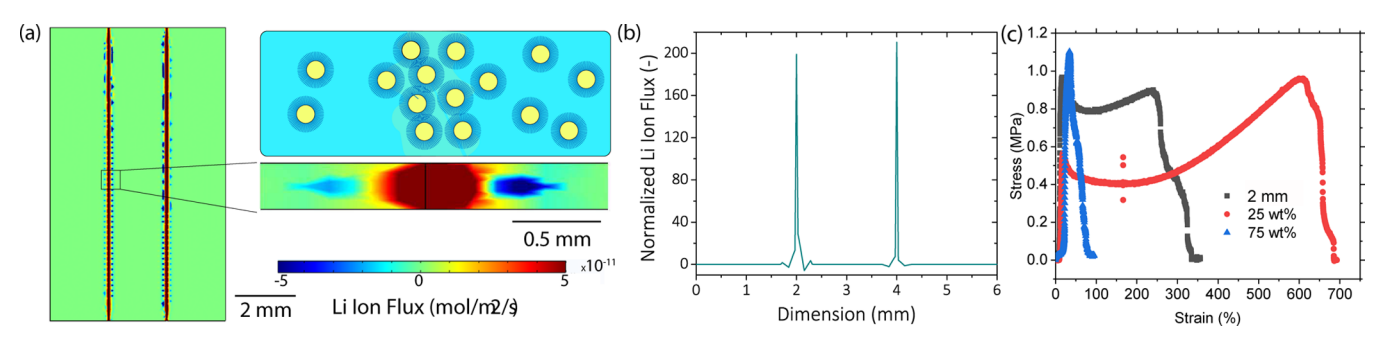


Figure 6. (a) Li ion flux distribution through a planar section of coextruded membrane. Flux at the interface along the transverse section is also shown. (b) Normalized Li ion flux across the width of the coextruded membrane studied using simulations. (c) Mechanical properties of singlematerial and coextruded films.

network that does not contribute to ion transport significantly. Moving to the single-material 75 wt % solid electrolyte demonstrates a shift in the relaxation time distribution curve toward smaller relaxation times (primary peak at 1×10^{-6} s) and a small shift of the peak at a higher relaxation time. The shift to lower relaxation times can be attributed to the modification of the polymer phase with the addition of the ceramic particles. Coextruded electrolytes all show a shift of peaks to lower relaxation times (primary peaks at 3.09×10^{-7} , 2.64×10^{-7} , and 7.64×10^{-7} s for CoX 1mm, CoX 2mm, and CoX 3mm, respectively), which suggest faster ion transport mechanisms (Figure 5c). Additionally, coextruded solid electrolytes have features at very low relaxation times (10^{-7} s) , which suggest that a region of fast transport exists in these samples.

While distribution of relaxation times helps to show the presence of interfacial regions with disparate ion transport properties, the physical properties of these regions are not quantifiable. Effective mean field theory (EMFT) was originally proposed by Bruggeman⁶⁵ to predict the effective properties of composite materials. The theory has been extensively improved since then and has been recently employed to screen mixture compositions for hybrid electrolytes. EMFT models use conductivity values for individual components of a composite matrix as well as the interface to predict the properties of the composite matrix (Figure 5b). We leverage this model and use it implicitly to solve for the interfacial properties. An assumption for very thin interfaces (compared to the particle radius) is taken to simplify the analysis. This approximation is fairly safe considering the length-scale interface layer is expected to propagate from the particle surface. We employ this model to predict the properties of macroscale interfaces generated in the coextruded

The interface in the 25 wt % system between the polymer phase and ceramic phase shows lower ionic conductivity than the polymer (55 °C) (Figure S6a). Ion transport would favor the polymer in this case and the ionic conductivity of the hybrid membrane falls close to the bare polymer. At temperature $\langle T_{\rm m} \rangle$, the hybrid electrolyte shows a slight improvement possibly due to the addition of the ceramic filler and a decrease in the polymer crystallinity. At temperatures above the melting temperature, the bulk polymer becomes amorphous, resulting in similar transport properties between each stripe. The interface is estimated to be more conducting $< T_{\rm m}$ for the 75 wt % system (Figure S6b). The increased particle loading leads to generation of interfacial regions in the vicinity of the particles that possess a locally amorphous

polymer structure and strong anion suppression. This results in the improved interfacial conductivity for this system. The interfacial conductivity shows a decay after 55 °C for the 75 wt % system. A higher ceramic loading in this system possibly restricts the polymer segmental motion, lowering the interfacial conductivity. The model predicts that the interfacial conductivity in a 1 mm striped coextruded electrolyte is higher than the ionic conductivity of the 25 and 75 wt % system $\langle T_{\rm m}$ (Figure 5d). The ionic conductivity of the interfacial layer for this configuration is slightly lower than the coextruded sample with smaller activation energies (Table 1). This suggests that the interfacial layer between the 25and 75 wt % sample possesses an improved ion transport pathway in the coextruded sample. A similar behavior is seen for the other coextruded samples (Figure 5e and Figure S6c,d). Electrolytes with 1 mm stripe architectures show the highest interfacial conductivity and lower activation energies.

The impact of the macrointerface on transport is further investigated using computational modeling. Steady-state concentration flux across a domain containing three stripes 2 cm wide and 60 μ m-thick is evaluated (top view seen in Figure 6a). The ion transport properties of two stripes are kept equal to that obtained for the 25 wt % system, while the center stripe is provided in the ion transport properties of the 75 wt % system. It should be noted that the hybrid electrolytes have been modeled as a uniform phase in these simulations. A small current density is applied across the top and bottom surface of the electrolyte domain. Steady-state ion transport simulations show strong localization of lithium ion flux at the interfacial region between the two material systems (Figure 6a). The cross section across the thickness of the electrolyte at the interface highlights the lithium ion distribution at the interfacial region for the coextruded architectures. Normalized flux averaged across the entire length of the simulated domain shows clear spikes in lithium ion flux at the interfacial region (Figure 6b). Simulations show an enhancement factor of ≈ 200 in the ion flux at the interfacial regions. Figure 6c demonstrates how the mechanical properties of the electrolyte are altered with the ceramic content and with coextrusion. The mechanical properties appear to obey superposition. The single-material 25 wt % ceramic/polymer electrolyte has the longest elongation at break (650%), and the 75 wt % ceramic/ polymer solid electrolyte has the shortest elongation at break (50%). The coextruded film, which is composed of both 25 and 75 wt % stripes, falls in between the single-material electrolyte and breaks at 300%.

4. CONCLUSIONS

A novel manufacturing platform for the scalable production of hybrid solid electrolytes is demonstrated. Coating hybrid solid electrolytes with structural and compositional variation at rollto-roll scales provide a pathway to engineer transport pathways on the fly. Herein, we demonstrate a novel architecture that introduces macrointerfaces into a polymer ceramic matrix. These interfaces demonstrate an increase in ion transport properties compared to single-material films. Detailed analysis of impedance data and modeling studies provide phenomenological insight into ion transport kinetics at these interfaces. Long-term control over ion transport properties and pathways is necessary to achieve uniform stripping and plating mechanisms with lithium metal anodes. This proof-of-concept study presents one potential manufacturing strategy to address this need. Achieving reliability in manufacturing is also identified as an important aspect toward commercialization of solid-state batteries.

ASSOCIATED CONTENT

S Supporting Information

The Supporting Information is available free of charge at https://pubs.acs.org/doi/10.1021/acsami.9b15463.

Additional experimental methods, description of EMFT model, additional modeling, and experimental results (PDF)

AUTHOR INFORMATION

Corresponding Author

*E-mail: kelsey.b.hatzell@vanderbilt.edu. Phone: +1 (615)-875-8391.

ORCID ®

Marta C. Hatzell: 0000-0002-5144-4969 Kelsey B. Hatzell: 0000-0002-5222-7288

Notes

The authors declare no competing financial interest.

ACKNOWLEDGMENTS

The authors were supported by the National Science Foundation under grant nos. 1727863 and 1727668. The authors acknowledge the Vanderbilt Institute of Nanoscience and Engineering (VINSE) for access to their shared characterization facilities. This research used resources of the Advanced Photon Source, a U.S. Department of Energy (DOE) Office of Science User Facility operated for the DOE Office of Science by Argonne National Laboratory under contract no. DE-AC02-06CH11357.

REFERENCES

- (1) Janek, J.; Zeier, W. G. A Solid Future for Battery Development. *Nat. Energy* **2016**, *1*, 16141.
- (2) Cheng, X.-B.; Zhang, R.; Zhao, C.-Z.; Zhang, Q. Toward Safe Lithium Metal Anode in Rechargeable Batteries: A Review. *Chem. Rev.* **2017**, *117*, 10403–10473.
- (3) Shen, F.; Dixit, M. B.; Xiao, X.; Hatzell, K. B. Effect of Pore Connectivity on Li Dendrite Propagation Within LLZO Electrolytes Observed with Synchrotron X-ray Tomography. ACS Energy Lett. 2018, 1056.
- (4) Sun, C.; Liu, J.; Gong, Y.; Wilkinson, D. P.; Zhang, J. Recent Advances in All-Solid-State Rechargeable Lithium Batteries. *Nano Energy* **2017**, *33*, *363*–386.

- (5) Zheng, F.; Kotobuki, M.; Song, S.; Lai, M. O.; Lu, L. Review on Solid Electrolytes for All-Solid-State Lithium-Ion Batteries. *J. Power Sources* **2018**, 389, 198–213.
- (6) Fan, L.; Wei, S.; Li, S.; Li, Q.; Lu, Y. Recent Progress of the Solid-State Electrolytes for High-Energy Metal-Based Batteries. *Adv. Energy Mater.* **2018**, 1702657.
- (7) Keller, M.; Varzi, A.; Passerini, S. Hybrid Electrolytes for Lithium Metal Batteries. *J. Power Sources* **2018**, 392, 206–225.
- (8) Liu, Q.; Geng, Z.; Han, C.; Fu, Y.; Li, S.; He, Y.-b.; Kang, F.; Li, B. Challenges and Perspectives of Garnet Solid Electrolytes for All Solid-State Lithium Batteries. *J. Power Sources* **2018**, 389, 120–134.
- (9) McCloskey, B. D. Attainable Gravimetric and Volumetric Energy Density of Li-S and Li Ion Battery Cells with Solid Separator-Protected Li Metal Anodes. *J. Phys. Chem. Lett.* **2015**, *6*, 4581–4588.
- (10) Zaman, W.; Hortance, N.; Dixit, M. B.; De Andrade, V.; Hatzell, K. B. Visualizing Percolation and Ion Transport in Hybrid Solid Electrolytes for Li-Metal Batteries. *J. Mater. Chem. A* **2019**, *7*, 23914–23921.
- (11) Zhang, X.; Liu, T.; Zhang, S.; Huang, X.; Xu, B.; Lin, Y.; Xu, B.; Li, L.; Nan, C.-W.; Shen, Y. Synergistic Coupling Between Li_{6.75}La₃Zr_{1.75}Ta_{0.25}O₁₂ and Poly(vinylidene fluoride) Induces High Ionic Conductivity, Mechanical Strength and Thermal Stability of Solid Composite Electrolytes. *J. Am. Chem. Soc.* **2017**, *139*, 13779–13785.
- (12) Tang, W.; Tang, S.; Zhang, C.; Ma, Q.; Xiang, Q.; Yang, Y.-W.; Luo, J. Simultaneously Enhancing the Thermal Stability, Mechanical Modulus, and Electrochemical Performance of Solid Polymer Electrolytes by Incorporating 2D Sheets. *Adv. Energy Mater.* **2018**, 1800866.
- (13) Liu, S.; Imanishi, N.; Zhang, T.; Hirano, A.; Takeda, Y.; Yamamoto, O.; Yang, J. Effect of Nano-Silica Filler in Polymer Electrolyte on Li Dendrite Formation in Li /poly(ethylene oxide)—Li(CF₃SO₂)₂N/Li. *J. Power Sources* **2010**, *195*, *6847*–*6853*.
- (14) Deka, M.; Kumar, A. Electrical and Electrochemical Studies of poly(vinylidene fluoride)—Clay Nanocomposite Gel Polymer Electrolytes for Li-Ion Batteries. *J. Power Sources* **2011**, *196*, 1358—1364.
- (15) Wu, X.-L.; Xin, S.; Seo, H.-H.; Kim, J.; Guo, Y.-G.; Lee, J.-S. Enhanced Li⁺ Conductivity in PEO–LiBOB Polymer Electrolytes by Using Succinonitrile as a Plasticizer. *Solid State Ionics* **2011**, *186*, 1–6.
- (16) Chen, X. C.; Sacci, R. L.; Osti, N. C.; Tyagi, M.; Wang, Y.; Palmer, M. J.; Dudney, N. J. Study of Segmental Dynamics and Ion Transport in Polymer–Ceramic Composite Electrolytes by Quasi-Elastic Neutron Scattering. *Mol. Syst. Des. Eng.* **2019**, *4*, 379–385.
- (17) Zheng, J.; Dang, H.; Feng, X.; Chien, P.-H.; Hu, Y.-Y. Li-Ion Transport in a Representative CeramicPolymerPlasticizer Composite Electrolyte: Li₇La₃Zr₂O₁₂–Polyethylene Oxide–Tetraethylene Glycol Dimethyl Ether. *J. Mater. Chem. A* **2017**, *5*, 18457–18463.
- (18) Zheng, J.; Hu, Y.-Y. New Insights into the Compositional Dependence of Li-Ion Transport in Polymer Ceramic Composite Electrolytes. ACS Appl. Mater. Interfaces 2018, 10, 4113–4120.
- (19) Zheng, J.; Tang, M.; Hu, Y.-Y. Lithium Ion Pathway within Li₇La₃Zr₂O₁₂–Polyethylene Oxide Composite Electrolytes. *Angew. Chem., Int. Ed.* **2016**, *SS*, 12538–12542.
- (20) Schnell, J.; Günther, T.; Knoche, T.; Vieider, C.; Köhler, L.; Just, A.; Keller, M.; Passerini, S.; Reinhart, G. All-Solid-State Lithium-Ion and Lithium Metal Batteries Paving the Way to Large-Scale Production. *J. Power Sources* **2018**, 382, 160—175.
- (21) Kerman, K.; Luntz, A.; Viswanathan, V.; Chiang, Y.-M.; Chen, Z. Review—Practical Challenges Hindering the Development of Solid State Li Ion Batteries. *J. Electrochem. Soc.* **2017**, *164*, A1731–A1744.
- (22) Bloomberg. *Lithium-ion Battery Costs and Market*. https://data.bloomberglp.com/bnef/sites/14/2017/07/BNEF-Lithium-ion-battery-costs-and-market.pdf (2017).
- (23) Chen, F.; Yang, D.; Zha, W.; Zhu, B.; Zhang, Y.; Li, J.; Gu, Y.; Shen, Q.; Zhang, L.; Sadoway, D. R. Solid Polymer Electrolytes Incorporating Cubic Li₇La₃Zr₂O₁₂ for AllSolid-State Lithium Rechargeable Batteries. *Electrochim. Acta* **2017**, 258, 1106–1114.
- (24) Langer, F.; Bardenhagen, I.; Glenneberg, J.; Kun, R. Microstructure and Temperature Dependent Lithium Ion Transport

- of Ceramic-Polymer Composite Electrolyte for SolidState Lithium Ion Batteries Based on Garnet-Type Li₇La₃Zr₂O₁₂. Solid State Ionics 2016, 291, 8-13.
- (25) Ban, X.; Zhang, W.; Chen, N.; Sun, C. A High-Performance and Durable Poly(ethylene oxide)-Based Composite Solid Electrolyte for All Solid-State Lithium Battery. J. Phys. Chem. C 2018, 122, 9852-9858
- (26) Wan, Z.; Lei, D.; Yang, W.; Liu, C.; Shi, K.; Hao, X.; Shen, L.; Lv, W.; Li, B.; Yang, Q.-H.; Kang, F.; He, Y.-B. Low Resistance-Integrated All-Solid-State Battery Achieved by Li₇La₃Zr₂O₁₂ Nanowire Upgrading Polyethylene Oxide (PEO) Composite Electrolyte and PEO Cathode Binder. Adv. Funct. Mater. 2019, 29, 1805301.
- (27) Zhu, L.; Zhu, P.; Yao, S.; Shen, X.; Tu, F. High-Performance Solid PEO/PPC/LLTO-Nanowires Polymer Composite Electrolyte for Solid-State Lithium Battery. Int. J. Energy Res. 2019, 43, 4854-4866.
- (28) Zhao, Y.; Yan, J.; Cai, W.; Lai, Y.; Song, J.; Yu, J.; Ding, B. Elastic and Well-Aligned Ceramic LLZO Nanofiber Based Electrolytes for Solid-State Lithium Batteries. Energy Storage Mater. 2019, 306.
- (29) Yang, T.; Zheng, J.; Cheng, Q.; Hu, Y.-Y.; Chan, C. K. Composite Polymer Electrolytes with Li₇La₃Zr₂O₁₂ Garnet-Type Nanowires as Ceramic Fillers: Mechanism of Conductivity Enhancement and Role of Doping and Morphology. ACS Appl. Mater. Interfaces 2017, 9, 21773-21780.
- (30) Li, Y.; Zhao, Y.; Cui, Y.; Zou, Z.; Wang, D.; Shi, S. Screening Polyethylene Oxide-Based Composite Polymer Electrolytes via Combining Effective Medium Theory and Halpin-Tsai Model. Comput. Mater. Sci. 2018, 144, 338-344.
- (31) Fu, K.; Gong, Y.; Dai, J.; Gong, A.; Han, X.; Yao, Y.; Wang, C.; Wang, Y.; Chen, Y.; Yan, C.; Li, Y.; Wachsman, E. D.; Hu, L. Flexible, Solid-State, Ion-Conducting Membrane with 3D Garnet Nanofiber Networks for Lithium Batteries. Proc. Natl. Acad. Sci. U. S. A. 2016, 113, 7094-7099.
- (32) Gürsoy, D.; De Carlo, F.; Xiao, X.; Jacobsen, C. TomoPy: A Framework for the Analysis of Synchrotron Tomographic Data. J. Synchrotron Radiat. 2014, 21, 1188-1193.
- (33) Schneider, C. A.; Rasband, W. S.; Eliceiri, K. W. NIH Image to ImageJ: 25 years of Image Analysis. Nat. Methods 2012, 9, 671-675.
- (34) Pandian, A. S.; Chen, X. C.; Chen, J.; Lokitz, B. S.; Ruther, R. E.; Yang, G.; Lou, K.; Nanda, J.; Delnick, F. M.; Dudney, N. J. Facile and Scalable Fabrication of Polymer-Ceramic Composite Electrolyte with High Ceramic Loadings. J. Power Sources 2018, 390, 153-164.
- (35) Chen, X. C.; Liu, X.; Samuthira Pandian, A.; Lou, K.; Delnick, F. M.; Dudney, N. J. Determining and Minimizing Resistance for Ion Transport at the Polymer/Ceramic Electrolyte Interface. ACS Energy Lett. 2019, 4, 1080-1085.
- (36) Tenhaeff, W. E.; Yu, X.; Hong, K.; Perry, K. A.; Dudney, N. J. Ionic Transport Across Interfaces of Solid Glass and Polymer Electrolytes for Lithium Ion Batteries. J. Electrochem. Soc. 2011, 158, A1143-A1149.
- (37) Li, Z.; Huang, H.-M.; Zhu, J.-K.; Wu, J.-F.; Yang, H.; Wei, L.; Guo, X. Ionic Conduction in Composite Polymer Electrolytes: Case of PEO:Ga-LLZO Composites. ACS Appl. Mater. Interfaces 2019, 11, 784-791.
- (38) Department of Energy. Roll to Roll Processing Technology Assessment; 2015.
- (39) Goda, T.; Sasaki, Y.; Mizuno, M.; Morizawa, K.; Katakura, H.; Tomiya, S. Numerical Analysis for Predicting the Operability Window of Slot-Die Coating Onto Porous Media. J. Coat. Technol. Res. 2017, 14, 1053-1060.
- (40) Ding, X.; Liu, J.; Harris, T. A. L. A Review of the Operating Limits in Slot Die Coating Processes. AIChE J. 2016, 62, 2508-2524.
- (41) Lee, S. H.; Koh, H. J.; Ryu, B. K.; Kim, S. J.; Jung, H. W.; Hyun, J. C. Operability coating windows and frequency response in slot coating flows from a viscocapillary model. Chem. Eng. Sci. 2011, 66, 4953-4959.

- (42) Ji, H. S.; Ahn, W.-G.; Kwon, I.; Nam, J.; Jung, H. W. Operability Coating Window of Dual-Layer Slot Coating Process Using Viscocapillary Model. Chem. Eng. Sci. 2016, 143, 122-129.
- (43) Maza, D.; Carvalho, M. S. Transient Response of Two-Layer Slot Coating Flows to Periodic Disturbances. AIChE J. 2015, 61,
- (44) Jin, G. L.; Ahn, W.-G.; Kim, S. J.; Nam, J.; Jung, H. W.; Hyun, J. C. Effect of Shim Configuration on Internal Die Flows for Non-Newtonian Coating Liquids in Slot Coating Process. J. Coat. Technol. Res. 2016, 28, 159-164.
- (45) Tsuda, T. Coating Flows of Power-Law Non-Newtonian Fluids in Slot Coating. Nihon Reoroji Gakkaishi 2010, 38, 223-230.
- (46) Nam, J.; Carvalho, M. S. Mid-Gap Invasion in Two-Layer Slot Coating. J. Fluid Mech. 2009, 631, 397-417.
- (47) Bhamidipati, K.; Didari, S.; Harris, T. A. L. Experimental Study on Air Entrainment in Slot Die Coating of High-Viscosity, Shear-Thinning Fluids. Chem. Eng. Sci. 2012, 80, 195-204.
- (48) Lee, Y. W.; Ahn, W.-G.; Nam, J.; Jung, H. W.; Hyun, J. C. Operability Windows in Viscoelastic Slot Coating Flows Using a Simplified Viscoelastic-Capillary Model. Rheol. Acta 2017, 707-717.
- (49) Han, G. H.; Lee, S. H.; Ahn, W.-G.; Nam, J.; Jung, H. W. Effect of Shim Configuration on Flow Dynamics and Operability Windows in Stripe Slot Coating Process. J. Coat. Technol. Res. 2014, 11, 19-29.
- (50) Lin, C.-F.; Wang, B.-K.; Lo, S.-H.; Wong, D. S.-H.; Liu, T.-J.; Tiu, C. Operating Windows of Stripe Coating. Asia-Pac. J. Chem. Eng. 2014, 9, 134-145.
- (51) Samanta, A.; Bera, A.; Ojha, K.; Mandal, A. Effects of Alkali, Salts, and Surfactant on Rheological Behavior of Partially Hydrolyzed Polyacrylamide Solutions. J. Chem. Eng. Data 2010, 55, 4315-4322.
- (52) Mohanty, D.; Hockaday, E.; Li, J.; Hensley, D. K.; Daniel, C.; Wood, D. L., III Effect of Electrode Manufacturing Defects on Electrochemical Performance of Lithium-Ion Batteries: Cognizance of the Battery Failure Sources. J. Power Sources 2016, 312, 70-79.
- (53) Heider, U.; Oesten, R.; Jungnitz, M. Challenge in Manufacturing Electrolyte Solutions for Lithium and Lithium Ion Batteries Quality Control and Minimizing Contamination Level. J. Power Sources 1999, 81-82, 119-122.
- (54) Brandt, K.; Laman, F. C. Reproducibility and Reliability of Rechargeable Lithium/Molybdenum Disulfide Batteries. J. Power Sources 1989, 265.
- (55) Shao, C.; Paynabar, K.; Kim, T. H.; Jin, J.; Hu, S. J.; Spicer, J. P.; Wang, H.; Abell, J. A. Feature Selection for Manufacturing Process Monitoring using CrossValidation. J. Manuf. Syst. 2013, 550.
- (56) Kurfer, J.; Westermeier, M.; Tammer, C.; Reinhart, G. Production of Large-Area Lithium-Ion Cells - Preconditioning, Cell Stacking and Quality Assurance. CIRP Ann. 2012, 1.
- (57) Ghosh, A.; Wang, C.; Kofinas, P. Block Copolymer Solid Battery Electrolyte with High Li-Ion Transference Number. J. Electrochem. Soc. 2010, 157, A846-A849.
- (58) Diederichsen, K. M.; McShane, E. J.; McCloskey, B. D. The Most Promising Routes to a High Li⁺ Transference Number Electrolyte for Lithium Ion Batteries. ACS Energy Lett. 2017, 2, 2563-2575.
- (59) Li, H.; Li, M.; Siyal, S. H.; Zhu, M.; Lan, J.-L.; Sui, G.; Yu, Y.; Zhong, W.; Yang, X. A Sandwich Structure Polymer/Polymer-Ceramics/Polymer Gel Electrolytes for the Safe, Stable Cycling of Lithium Metal Batteries. J. Membr. Sci. 2018, 555, 169-176.
- (60) Zhao, C.-Z.; Zhang, X.-Q.; Cheng, X.-B.; Zhang, R.; Xu, R.; Chen, P.-Y.; Peng, H.-J.; Huang, J.-Q.; Zhang, Q. An Anion-Immobilized Composite Electrolyte for Dendrite-Free Lithium Metal Anodes. Proc. Natl. Acad. Sci. U. S. A. 2017, 114, 11069-11074.
- (61) Doyle, M.; Fuller, T. F.; Newman, J. The Importance of the Lithium Ion Transference Number in Lithium/Polymer cells. Electrochim. Acta 1994, 39, 2073-2081.
- (62) Kim, S. U.; Srinivasan, V. A Method for Estimating Transport Properties of Concentrated Electrolytes from Self-Diffusion Data. J. Electrochem. Soc. 2016, 163, A2977-A2980.
- (63) Wan, T. H.; Saccoccio, M.; Chen, C.; Ciucci, F. Influence of the Discretization Methods on the Distribution of Relaxation Times

Deconvolution: Implementing Radial Basis Functions with DRTtools. *Electrochim. Acta* **2015**, *184*, 483–499.

- (64) Mertens, A.; Yu, S.; Schön, N.; Gunduz, D. C.; Tempel, H.; Schierholz, R.; Hausen, F.; Kungl, H.; Granwehr, J.; Eichel, R.-A. Superionic Bulk Conductivity in Li_{1.3}Al_{0.3}Ti_{1.7}(PO₄)₃ Solid Electrolyte. *Solid State Ionics* **2017**, 309, 180–186.
- (65) Bruggeman, D. A. G. Berechnung Verschiedener Physikalischer Konstanten von Heterogenen Substanzen. III. Die Elastischen Konstanten der Quasiisotropen Mischkörper aus Isotropen Substanzen. Ann. Phys. 1937, 421, 160–178.